

# Supplementary Material for

## Sr-doped SmMnO<sub>3</sub> Perovskites for High-performance Near-isothermal Solar Thermochemical CO<sub>2</sub>-Fuel Conversion

Ke Gao<sup>1</sup>, Chen Sun<sup>1</sup>, Xianglei Liu<sup>1\*</sup>, Tong Wang<sup>1</sup>, Zhonghui Zhu<sup>1</sup>, Ping Li<sup>1</sup>, Hangbin Zheng<sup>1</sup>, Yimin Xuan<sup>1</sup>, Yongliang Li<sup>2</sup>, Yulong Ding<sup>2</sup>

<sup>1</sup> School of Energy and Power Engineering, Nanjing University of Aeronautics and Astronautics, Nanjing 210016, China

<sup>2</sup> Birmingham Centre for Energy Storage, School of Chemical Engineering, University of Birmingham, Birmingham B15 2TT, UK

\*Corresponding author, E-mail: [xliu@nuaa.edu.cn](mailto:xliu@nuaa.edu.cn)

### The Word file includes:

Fig. S1 Thermodynamics for CO<sub>2</sub> splitting and H<sub>2</sub>O splitting.

Fig. S2 X-ray diffraction patterns of the cycled Sr-doped SmMnO<sub>3</sub>.

Fig. S3 DFT calculation of metal-oxygen strength.

Fig. S4 Temporal evolution of non-stoichiometric oxygen over time.

Fig. S5 Particle size distribution of as-synthesized Sr-doped SmMnO<sub>3</sub> and CeO<sub>2</sub>.

Fig. S6 Particle size distribution of cycled Sr-doped SmMnO<sub>3</sub> and CeO<sub>2</sub>.

Fig. S7 Particle size distribution of Sm<sub>0.6</sub>Sr<sub>0.4</sub>MnO<sub>3</sub> under different reaction conditions.

Fig. S8 Total CO<sub>2</sub> conversion rate for Sm<sub>0.6</sub>Sr<sub>0.4</sub>MnO<sub>3</sub> in 14 cycles.

Fig. S9 Temperature varies with the concentration ratio for remaining samples.

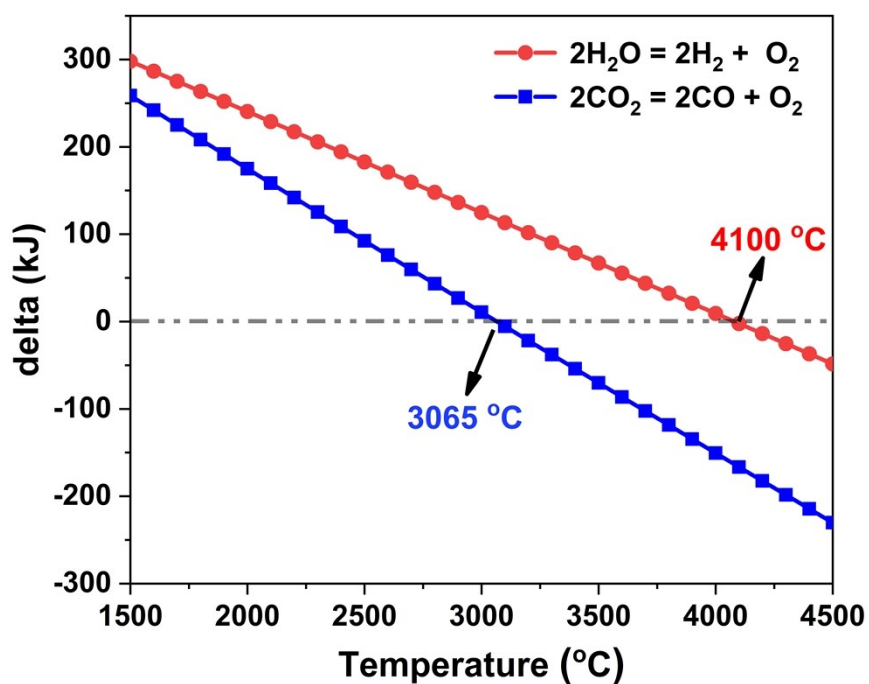


Fig. S1 Thermodynamics for  $\text{CO}_2$  splitting and  $\text{H}_2\text{O}$  splitting.

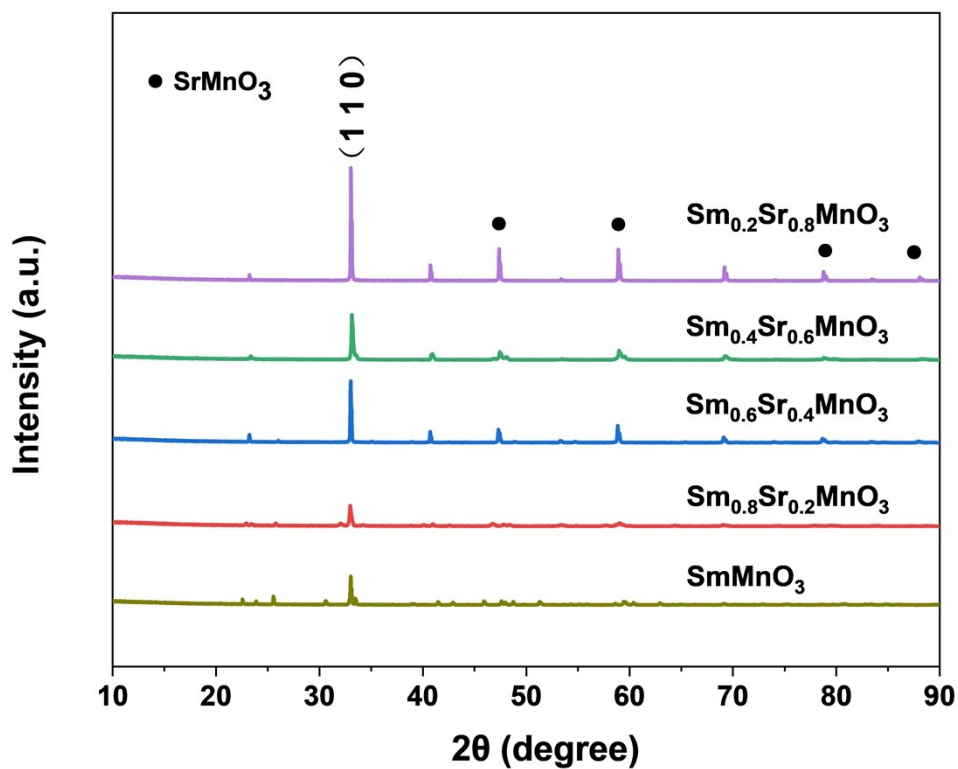


Fig. S2 X-ray diffraction patterns of the cycled Sr-doped  $\text{SmMnO}_3$ .

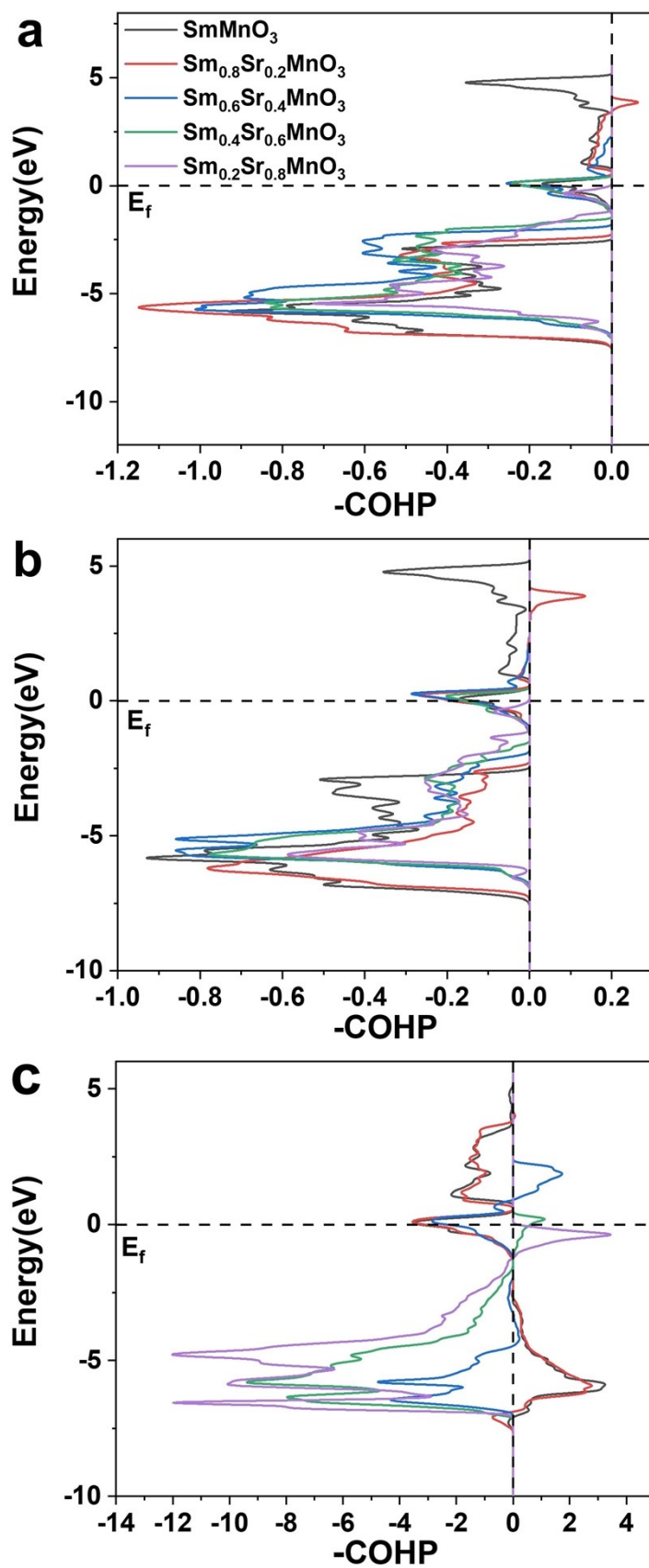


Fig. S3 DFT calculation of bond strength of (a) Sm-O, (b) Sr-O, and (c) Mn-O.

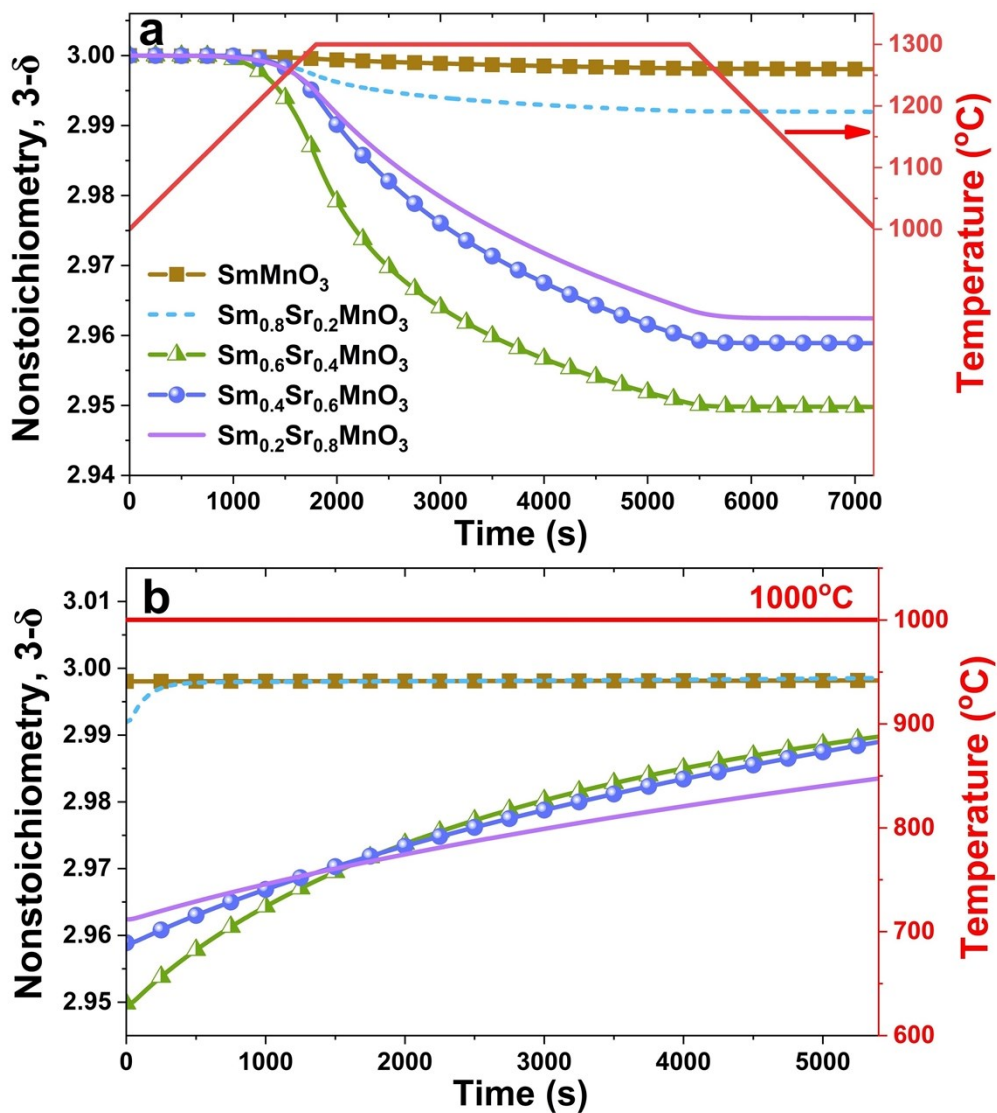


Fig. S4 Temporal evolution of non-stoichiometric oxygen over time during (a) reduction and (b) oxidation processes in the 2<sup>nd</sup> redox 1300  $^{\circ}\text{C}$  /1000  $^{\circ}\text{C}$  cycle.

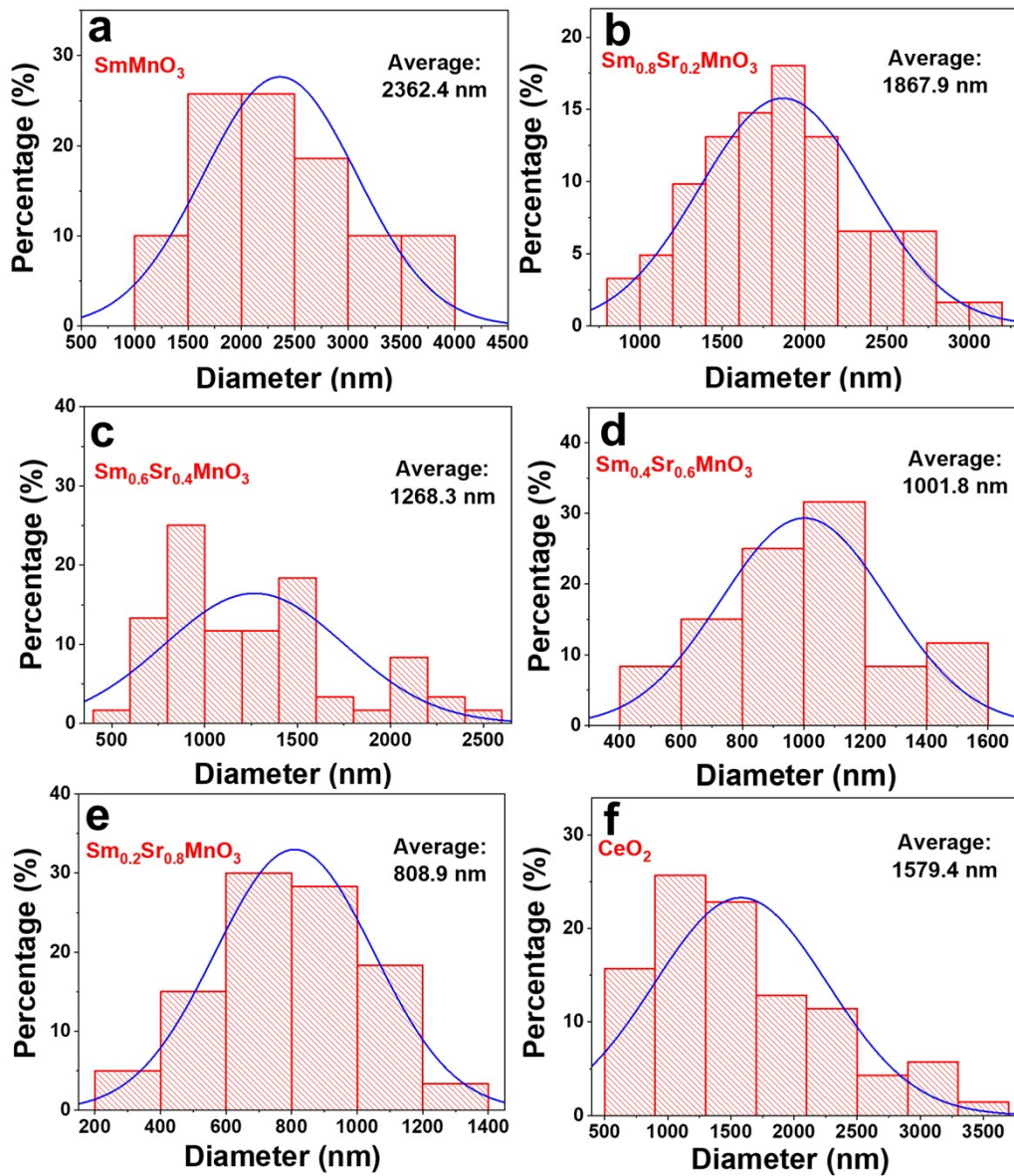


Fig. S5 Particle size distribution of as-synthesized Sr-doped  $\text{SmMnO}_3$  and  $\text{CeO}_2$  at 1300 °C/ 1000 °C redox cycle.

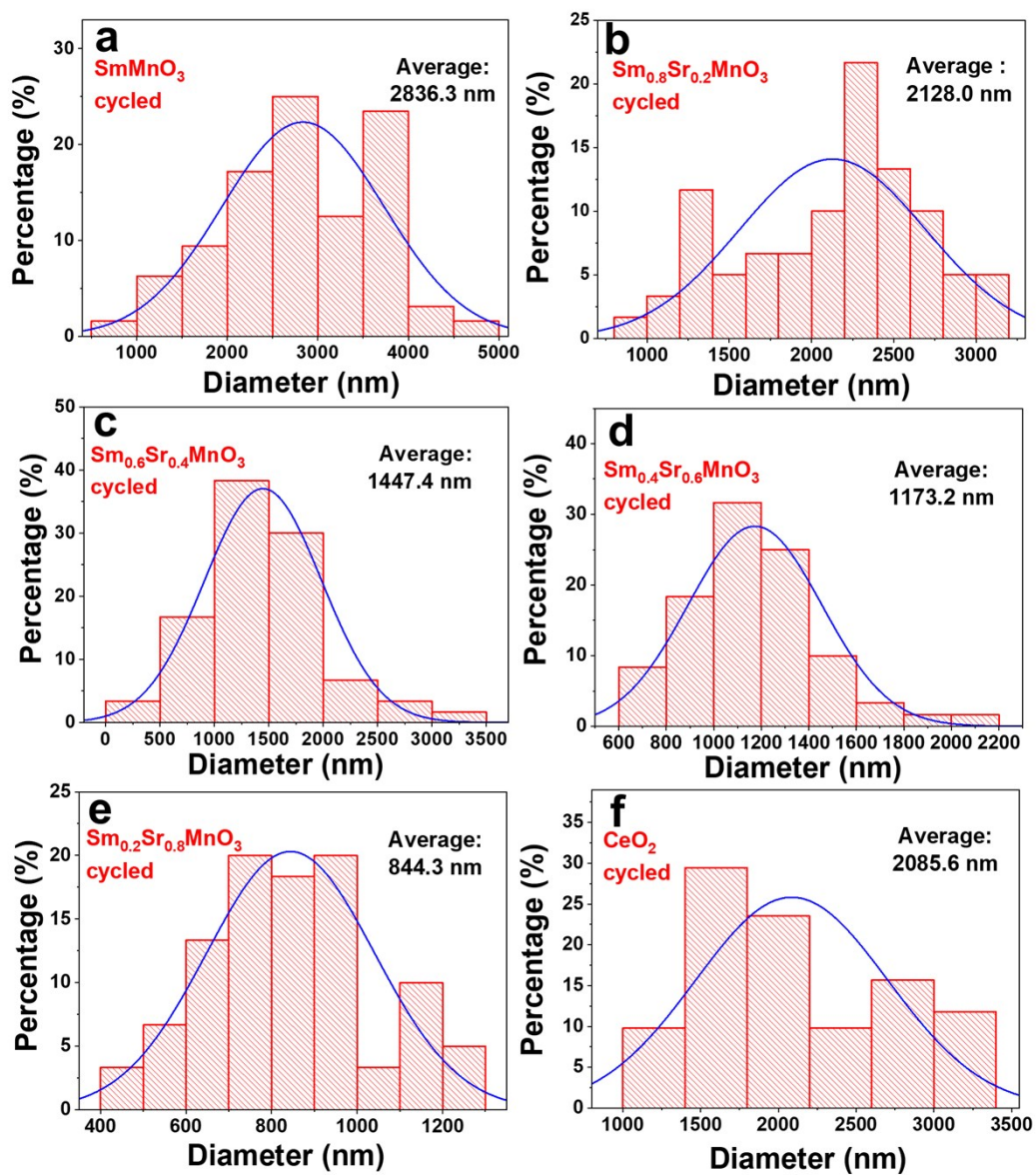


Fig. S6 Particle size distribution of cycled Sr-doped  $\text{SmMnO}_3$  and  $\text{CeO}_2$  at 1300 °C/ 1000 °C redox cycle.

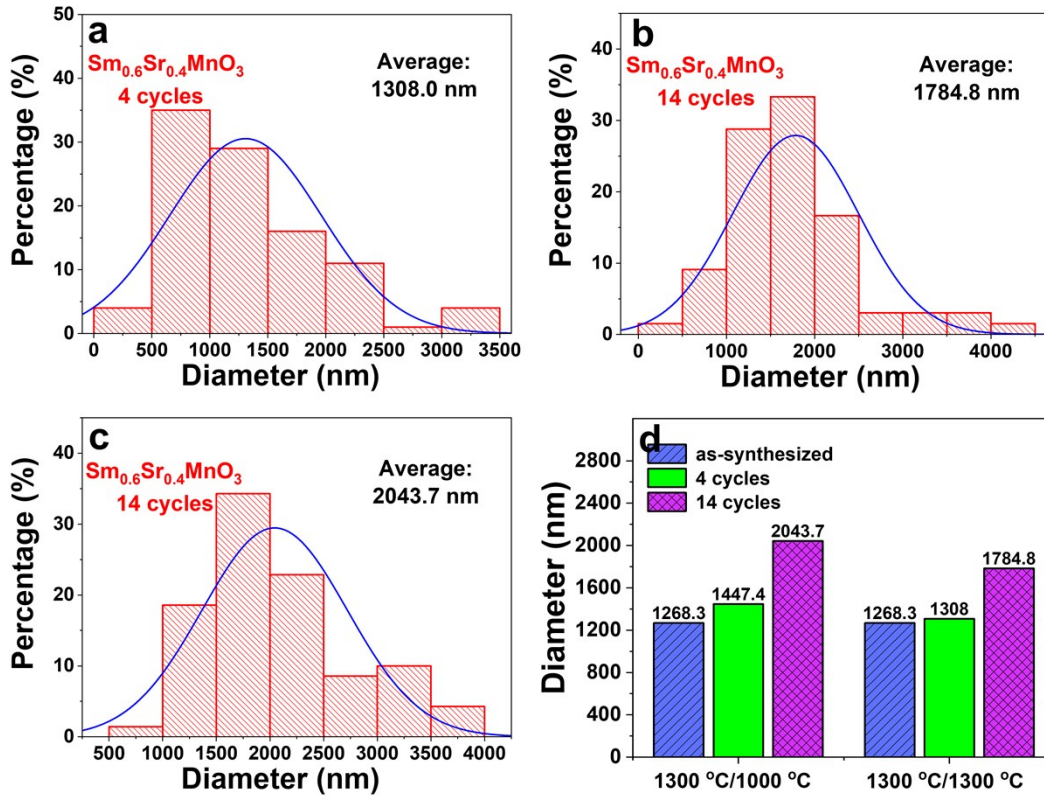


Fig. S7 Particle size distribution of  $\text{Sm}_{0.6}\text{Sr}_{0.4}\text{MnO}_3$  after a) 4 cycles and b) 14 cycles at 1300 °C/ 1300 °C and c) after 14 cycles at 1300 °C/ 1000 °C. d) The change of particle size for  $\text{Sm}_{0.6}\text{Sr}_{0.4}\text{MnO}_3$  after 0, 4, and 14 cycles at 1300 °C/ 1000 °C and 1300 °C/ 1300 °C.

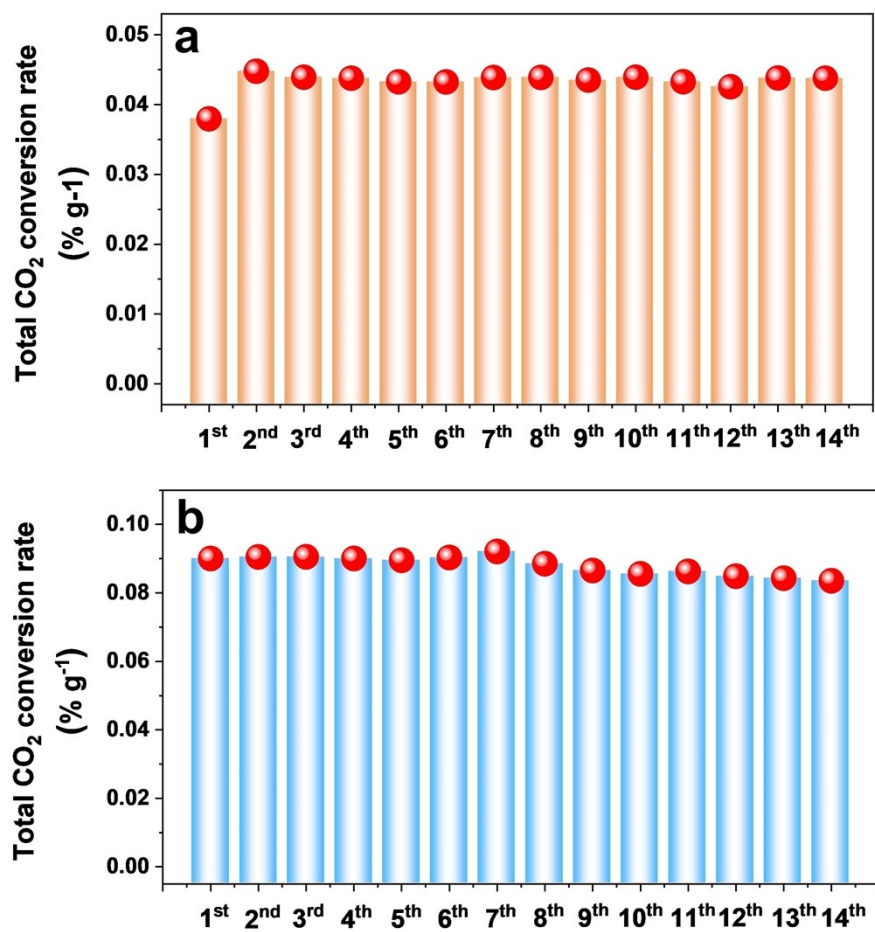


Fig. S8 Total CO<sub>2</sub> conversion rate for Sm<sub>0.6</sub>Sr<sub>0.4</sub>MnO<sub>3</sub> in 14 cycles at (a) 1300 °C/1000 °C and (b) 1300 °C/1300 °C redox reaction.

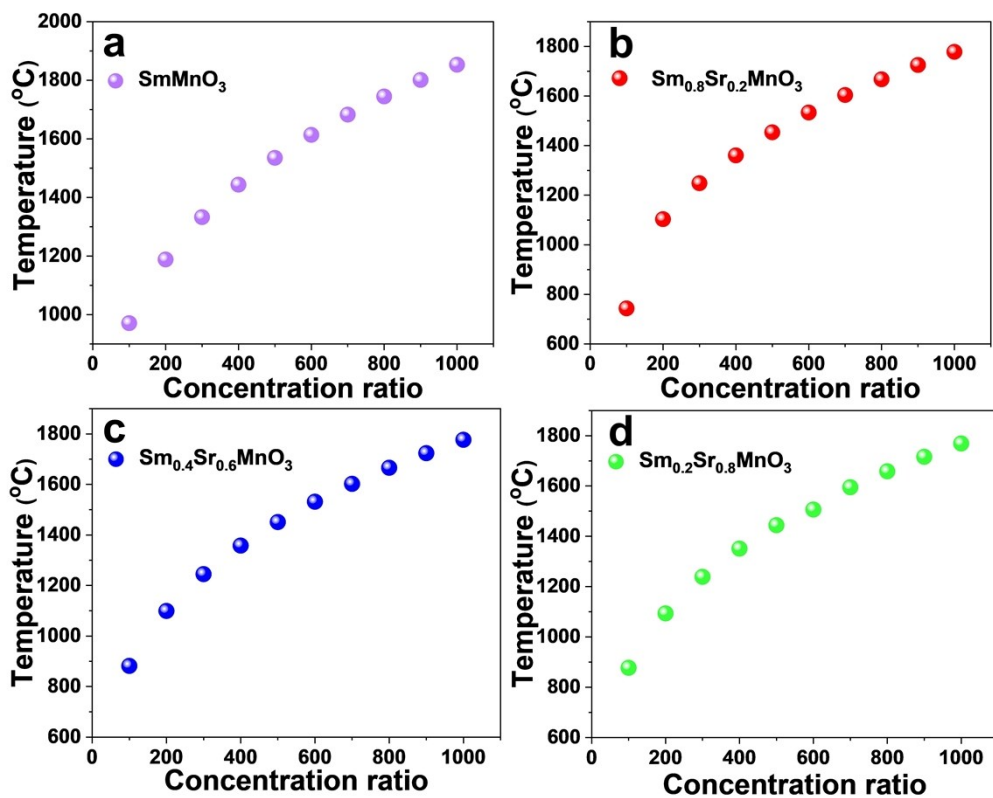


Fig. S9 Temperature varies with the concentration ratio for remaining samples.